A Sensitivity Assessment Framework for Frequency Ratio-Based Landslide Susceptibility Models: Evaluating the Role of Data Classification and Zonation

Salleh, H. A.,* **Abdul Rahman, E. K. and Ratnayake, U.**
Faculty of Engineering, Universiti Teknologi Brunei, Tungku Highway, Gadong, BE1410, Bandar Seri Begawan, Negara Brunei Darussalam
E-mail: hamirolaqim@gmail.com,* ena@utb.edu.bn, uditha.ratnayake@utb.edu.bn
Corresponding Author

DOI: https://doi.org/10.52939/ijg.v21i9.4441

Abstract
Landslide Susceptibility (LS) maps are essential tools for hazard assessment, yet the reliability of such maps is highly sensitive to methodological choices in data classification and discretisation. Although Frequency Ratio (FR) modelling is widely applied in LS assessments, limited research has systematically evaluated how the selection of classification techniques and classification schemes affects the accuracy and zoning of Landslide Susceptibility Index (LSI) outputs. This study proposes a sensitivity assessment framework that analyses the influence of four standard classification methods Natural Breaks, Quantile, Geometrical, and Equal Intervals under varying classification levels (4, 6, and 8 classes) on Frequency ratio-based LS modelling. Applied to two landslide-prone regions in Brunei Darussalam, the framework reveals that classification choices significantly alter predictive performance, map zoning, and model Receiver Operating Characteristic (ROC)-Area Under the Curve (AUC) rates (AUC=88%–97.7%). Of the 12 scheme–class-count combinations tested, a Geometrical-interval scheme with six classes gave the highest AUC (97.7 %) in the Kota Batu–Subok study areas, while a Quantile scheme with six classes was best for Jangsak–Tutong (AUC = 94.6 %). The framework is demonstrated on two rainfall-triggered hillslope study areas near Bandar Seri Begawan, Brunei Darussalam: Jalan Kota Batu–Subok (≈ 53 km²; 134 mapped debris-fall events) and Jalan Jangsak–Tutong (≈ 41 km²; 115 events), where steep sandstone–shale terrain and intense monsoon downpours routinely initiate shallow slides. We further show that varying classification can distort susceptibility zoning, potentially leading to misinformed risk decisions. These findings underscore the critical need for further investigation of classification methods in landslide modelling workflows and provide a reproducible method to reduce model uncertainty. Reproducibility is achieved through shareable ArcGIS ModelBuilder scripts and companion Excel templates that automate factor re-classification, frequency-ratio weighting, and fixed-seed validation, enabling any user with standard ArcGIS and Excel to recreate the maps and uncertainty metrics. The frequency-ratio probability maps allow planners to set evidence-based no-build buffers, rank slopes for stabilization works, and calibrate local rainfall-threshold warning systems, directly linking the research to real-world hazard mitigation.

Keywords: Area Under the Curve, Frequency Ratio, Hazards, Landslides Susceptibility, Receiver Operating Characteristic

1. Introduction

Landslide mapping is a foundational component of geohazard assessment and risk reduction. Among the most widely adopted approaches, the FR method offers a simple yet effective means of modelling spatial susceptibility based on historical landslide occurrences and conditioning factors [1] and [2]. However, a persistent blind spot in FR applications is the classification of continuous predictors the step that converts raw slope, elevation, or Stream Power Index (SPI) raster data into classified layers on which FR weights are calculated. Continuous terrain raster must be discretised before FR weights can be calculated. The four algorithms embedded in most GIS packages Natural Breaks, Quantile, Geometrical Interval and Equal Interval partition the same data in fundamentally different ways.

Natural Breaks minimises within-class variance, isolating dense value clusters; Quantile forces an equal pixel count per class, dampening extremes; Geometrical Interval applies a constant ratio, suiting log-skewed variables; and Equal Interval splits the range into uniform widths, ignoring distribution shape. Because FR weights are ratios of "landslide pixels" to "all pixels" within each class, shifting a single boundary changes both the numerator and the denominator, propagating into LS maps and $ROC - AUC$ scores. Most practitioners default to the four classification algorithms embedded in mainstream Geographical Information System (GIS) software Natural Breaks, Quantile, Geometrical Interval, and Equal Interval [3][4] and [5], without evidence-based guidance on which algorithm (and how many classes) best preserves the underlying landslide susceptibility. Recent studies from India, Türkiye, and Europe have shown that switching among standard classification schemes can shift the AUC by 8–15 % points and relocate high-risk zones by up to 20% [5][6] and [7]. Despite these stakes, a systematic, location-specific sensitivity assessment of classification effects on FR results is still missing from the literature.

To close this gap, this study designs a reproducible ArcGIS-based workflow that benchmarks 12 scheme class-count combinations across two contrasting, landslide susceptible study areas near Bandar Seri Begawan: Jalan Kota Batu–Subok (≈ approximately 53 km², 134 mapped debris-fall events) and Jalan Jangsak–Tutong (≈ approximately 41 km², 115 events). By comparing ROC-AUC analysis of FR and prediction weight distributions concerning zonation schemes and optimal ROC-AUC outcomes, and zonation overlap for each combination, this study (i) quantifies how classification choices propagate into FR weights distribution and Landslide-Susceptibility-Index (LSI) zoning, and (ii) identify the context in which a given scheme is optimal or detrimental. The findings show that classification is not a neutral preprocessing step but a determinative modelling choice, and they culminate in practical recommendations for hazard managers who rely on FR maps to prioritise slope-stabilisation works and calibrate rainfall-threshold warnings.

2. Methodology

2.1 Study Area

The proposed methodology was applied to the Jalan Kota Batu-Subok and Jalan Jangsak-Tutong areas located on the northeast and southwest sides of Bandar Seri Begawan, Brunei Darussalam, which spread over 53.40Km^2 and 40.80 km^2 (Figure 1). Between 2008 and 2018, Jalan Kota Batu-Subok and Jalan Jangsak-Tutong each recorded 134 and 115 landslides, respectively, which is the highest record in the region [8]. The bulk of the soil on Jalan Jangsak-Tutong is very thick, light brown, silty fine to medium sand. In contrast, the soil on Jalan Kota Batu-Subok is fine, dark greyish brown, mottled with red and yellow, sandy, silty clay, bedded with sandstone rocks. The central portion of landslides in these case studies was caused by debris falls [9] and as seen in both Figure 2 and Figure 3.

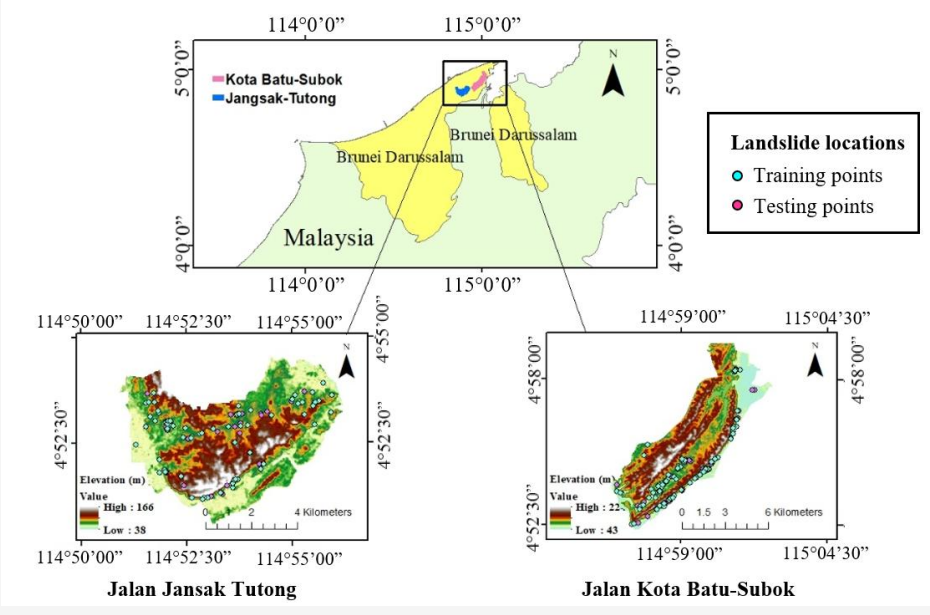

Figure 1: Map of the study areas showing elevations and landslide locations

Figure 2: Landslide with debris near a residential area at Jalan Kota Batu, Kg Dato Gandi, Brunei Muara [10]

Figure 3: Landslide occurrence near a commercial building at Jalan Tutong of Kampong Madewa, Mukim Kilanas, Brunei Muara [10]

Most of the landslides occurred near developed areas. On Jalan Jangsak-Tutong, a developed area is about 3.44 km^2, and on Jalan Kota Batu-Subok, a developed area is about 3.26 km^2. Most of the built-up areas are near the slopes and at the base of the hills. Both study areas are heavily populated, with a closely packed residential and commercial development positioned near or on the slopes, making the sites highly relevant for hazard management. This mix of geology, topography, and intense built-up pressure provides a rigorous test bed for classification-sensitivity analysis while keeping data resolution and mapping scale uniform.

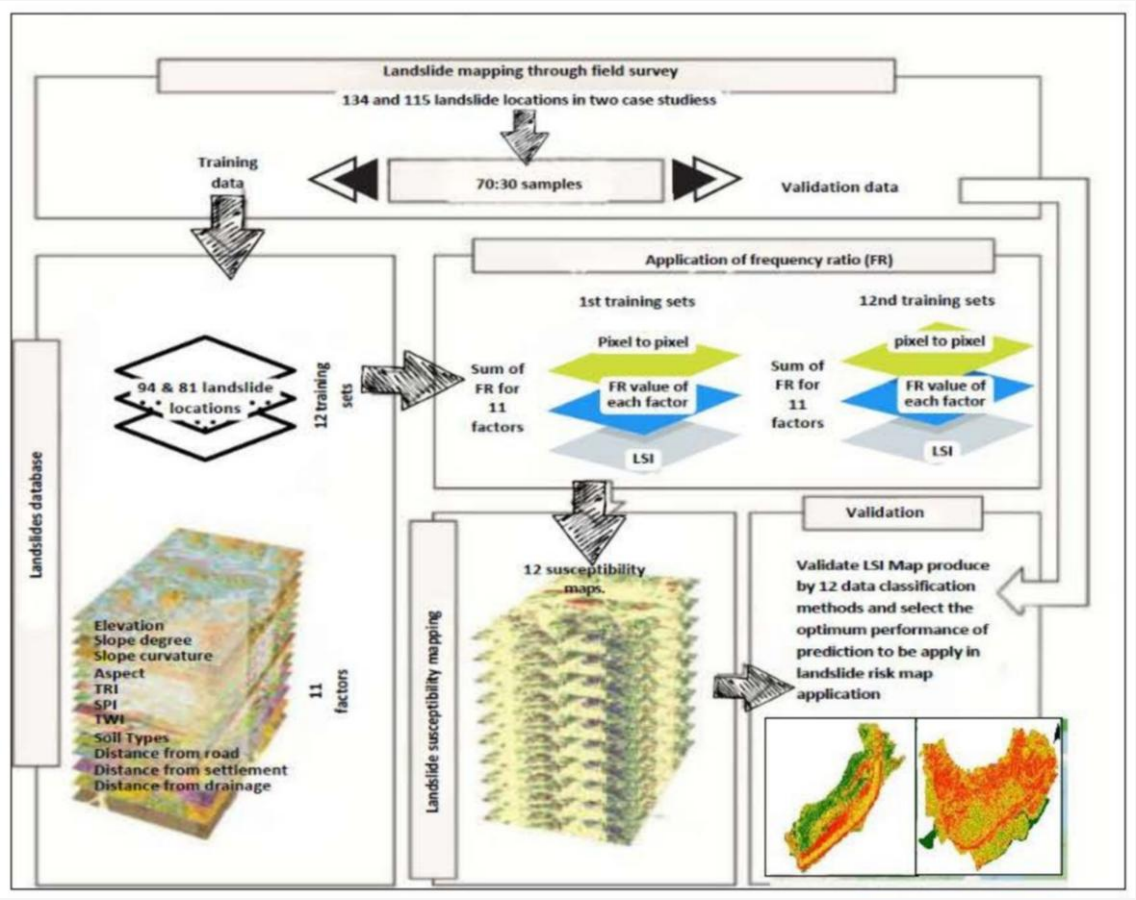

Figure 4: Workflow of the landslide-susceptibility (LS) assessment carried out in this study

2.2 Framework

This study employs an open, five-stage workflow applied to two case study areas (see Figure 4): Jalan Kota Batu–Subok (53 km²; 134 mapped debris-fall events) and Jalan Jangsak–Tutong (41 km²; 115 events). First, each landslide inventory was randomly partitioned into 70% training and 30% validation subsets. Second, eleven conditioning rasters elevation, slope, profile curvature, aspect, Topographic ruggedness index (TRI), SPI, Topographic wetness index (TWI), soil type, and distances to roads, settlements, and drainage were resampled to a 12.5m grid. Third, each continuous raster layers were discretised using twelve alternatives (Natural Breaks, Quantile, Geometrical, and Equal Interval at 4, 6, and 8 classes). Fourth, pixel-by-pixel FR weights were computed for every scheme–class combination, including the non-continuous factors (e.g., Aspect, curvature and soil type) and summed to generate twelve preliminary LS maps per corridor. Fifth, the withheld 30 % of landslides were used to calculate $ROC - AUC$ and prediction-rate statistics, rank all maps, and identify the highest-performing classification for each study area.

2.3 Landslide Conditioning Factors

Of the total 134 (Jalan Kota Batu-Subok landslides record) and 115 (Jalan Jangsak Tutong landslides record) landslides in the inventory map, 70% were randomly selected for the training dataset, and the remaining 30% were allocated to the testing dataset using ArcGIS random sampling tools. Landslide conditioning factors in Table 1 were used to produce *LSI* for the case studies. The factors comprised both continuous and categorical data types. Continuous data, for example, slope angle, can take on any value within a finite interval, whereas categorical data were distinct as different soil types, aspect and curvature. Conditional factors for landslides are represented in the spatial raster data format. The Digital Elevation Model (DEM) data was sourced from the open-source NASA Earth data, utilizing the Alaska Satellite Facility's (ASF) data search vertex portal, with a resolution of 12.5m [11].

Table 1: Landslide conditional factors used to assess landslide susceptibility

Landslide conditional factors	Type	Data range/group
Aspect	Categorical	Flat North Northeast East Southeast South Southwest West Northwest North
Curvature	Categorical	Concave Flat Convex
Distance from drains (m)	Continuous	0 - 1094.32
Distance from roads (m)	Continuous	0 - 2442.85
Distance from settlements (m)	Continuous	0 - 925.81
Soil type	Categorical	Nyalau (NY) Rajang (RG) Pendam (PD) Sebandi/Bijat (SB/BJ) Tatau (TA) Nyalau/Kapit (NY/KP) Merit/Malang (ME/MA) Mukah (MU) Malang/Bijat (MA/BJ) Malang (MA) Bekenu/Nyalau (BK/NY) Bijat (BJ)
SPI	Continuous	0 - 12573.19
TRI	Continuous	0 - 29.11
TWI	Continuous	1.04 - 11.74
Elevation (m)	Continuous	43 - 224
Slope angle (degree)	Continuous	0 - 77.24

The DEM data layer was utilized to generate the slope angle, curvature, aspect, TRI, TWI, and SPI in the ArcGIS system. Meanwhile, the Euclidean distance was calculated for existing settlements, roads, and drainage within the study areas through the Euclidean tool in ArcGIS. The base information was obtained from the Geotechnical Unit of the Public Works Department in Brunei, which was subsequently used to establish a polygon layer in the GIS. A "local evidence & transferable best-practice" strategy was applied. First, the variables that proved most effective in the original Jalan Kota Batu study slope, elevation, profile curvature, aspect, SPI, TRI, TWI, soil type, and Euclidean distances to roads, drainage, and settlements were retained, as they demonstrated predictive power in the identical litho-stratigraphic and climatic setting and are available at 12.5m resolution for both case studies [12]. Second, the list was cross-checked against recent FR research that highlights the same factors as the most influential in tropical and monsoon terrains [1][4] [13][14] and [15]. Factors excluded were lithology (minimal contrast across the study area), Normalized Difference Vegetation Index (NDVI) (cloud masking left > 25 % missing pixels), and gridded rainfall (due to a significant gap in rainfall records for the case studies). The final eleven-factor set, therefore, balances demonstrated local efficacy, international best practice, and practical data-quality constraints.

Table 2: Surface Soil Types information with thickness average and range details from Jalan Kota Batu Subok and Jalan Jangsak Tutong

Soil Codes	Type	Soil composition	Thickness of surface-soil layer (m)
NY	Nyalau	Fine dark greyish brown mottled with red and yellow sandy, silty CLAY bedded with sandstone boulder (filled materials)	7.2
RG	Rajang	Very soft dark greyish-brown peaty clay with decomposed vegetation and clayey silt	3-16
PD	Pendam	Loose greyish brown fine silty sand with peats	3.6
SB/BJ	Sebandi/Bijat	Soft dark brown clayey SILT with root/Firm to stiff yellowish-brown clayey SILT/Very stiff mottled yellowish-brown and grey silty CLAY/Hard dark grey silty CLAY	5.5
TA	Tatau	Stiff grey mottled with yellow sandy, silty CLAY with roots and decayed vegetation/Very soft yellowish-grey silty sandy CLAY/Very soft brownish grey sandy silty CLAY with organic matter	4.5
NY/KP	Nyalau/Kapit	Very soft yellowish-brown CLAY thinly laminated with fine silty sand and roots/Firm dark grey mottled with brown CLAY thinly laminated with silty fine sand/Firm dark grey with spots of brown CLAY thinly laminated with fine silty sand	6.0
ME/MA	Merit/Malang	Loose brownish and some fine grey sandy, clayey SILT/Soft and firm dark grey silty CLAY and some SILT/Loose brown-yellow silty excellent SAND	4.8
MU	Mukah	Very soft brown sandy CLAY, firm greyish brown silty CLAY	2.56
MA/BJ	Malang/Bijat	Soft brown mottled with orange sandy CLAY with roots, loose brownish yellow silty SAND, very soft brownish grey silty CLAY	5.7
MA	Malang	Very soft dark brown clayey SILT with traces of decayed vegetation and sand	3.0
BK/NY	Bekenu/Nyalau	Very dense light brown silty fine to medium SAND	5.0
BJ	Bijat	Very loose yellowish-brown silty SAND with decayed wood	1.5

In addition, the determination of surface soil types depended on a polygon shapefile provided by the Agricultural Department of Brunei Darussalam, supplemented with soil drilling data obtained from the Geotechnical Section of the Brunei Public Works Department (see Table 2). Soil type (in Table 2) is a significant determinant in the susceptibility to landslides. Various soil types exhibit different physical characteristics, including permeability, cohesion, and frictional resistance. These properties influence how soil types react to specific conditions, such as intense rainfall or seismic activity, which are common triggers for landslides [16] and [17]. In Brunei, during extreme rainfall events, some types of soil, despite having intact vegetation cover, are incapable of preventing structural failure, resulting in phenomena such as collapsing trees. This is particularly prevalent in clay-rich soils that have a high capacity for water absorption. The excess water reduces the shear strength of these soils, leading to their failure [9]. In this study, the soil type data, initially in polygon format, were rasterized to a 12.5m resolution.

2.4 Data Classification and Interval Methods

Eight landslide conditional factors (excluding Soil type, Curvature, and Aspect due to fixed class of categorical/ordinal data) with continuous data type were classified with different data classification methods as described below, whereby each method adopted 4, 6, and 8 classes, which were termed factor classes using an ArcGIS reclassified tool:

1. Natural breaks: class boundaries were set based on relatively big jumps in the observation count.

2. Quantile breaks: boundaries define classes containing an equal number of observation counts.
3. Geometrical breaks: class intervals form a geometric series while minimizing the sum of squares of the observation count in each class.
4. Equal intervals: boundaries with equal class range intervals.

The choice of classification methods and intervals in landslide susceptibility mapping and prediction plays a crucial role in accurately representing and interpreting the results. Different classification methods can lead to different visual patterns, sometimes in a distorted or biased manner [18]. The choice of maximum and minimum class boundaries can strongly affect the visual impression given by a map [19]. Class intervals can vary depending on the degree of uniformity in the numerical array being classified for mapping, with smaller intervals in the modal portions of a distribution and larger intervals in the tails. It is important to note that the choice of class intervals and methods can significantly impact the results of landslide susceptibility mapping. Different classification methods and interval selection techniques can lead to variations in the spatial patterns and interpretations of susceptibility maps [20]. Table 3 summarizes the statistical rationale, chief advantages, and key limitations of each method, helping to investigate which scheme best fits their data and mapping objective. Therefore, researchers should carefully consider the characteristics of the data and the study's objectives when selecting class intervals for landslide susceptibility mapping and prediction. Hence, the study seeks to examine how different classification approaches influence the LSI outcomes. Cartographic cognition studies show that map readers reliably discriminate about five to nine colour categories before confusion rises sharply [21] and [22]. Staying within that perceptual window, most recent LS papers benchmark classification sensitivity with totals in the same range- e.g. another study tested five classes with AUC >80% [22] and [1], some studies used eight classes [23], and reported diminishing AUC <70% gains beyond eight classes. On this empirical and practical basis, we adopted the even sequence 4–6–8, balancing visual clarity, alignment with current practice, and avoidance of data-sparsity artefacts.

Table 3: Comparative summary of the four GIS-default classification algorithms Natural Breaks, Quantile, Geometrical Interval, and Equal Interval highlighting their main advantages, and typical limitations

Method	Advantages	Limitations
Natural Breaks (Jenks)	• Captures real data groupings • Produces intuitive class boundaries on skewed data	• Class widths are irregular → difficult to compare between studies • Very narrow top classes can inflate FR weights and overstate hazard
Quantile	• Ensures balanced sample sizes for FR statistics • Easy to implement and interpret	• Can "dilute" extreme values into the same class as moderate ones, masking steep-slope hazards • Class breaks depend on the study area's extent, limiting transferability
Geometrical Interval	• Handles highly skewed or log-normal variables (e.g., drainage density) • Smooth, predictable break sequence	• Over-emphasises the upper tail if the data are not truly log-distributed • Requires careful choice of starting minimum
Equal Interval	• Simple, transparent boundaries • Facilitates cross-study comparison when variable ranges are similar	• Ignores data clustering; classes may be under- or over-populated • Extreme values can dominate the top class, dampening contrast in FR weights

2.5 FR Model

The FR approach determines the bivariate relationships between landslide occurrence and landslide conditional factors [24]. Therefore, after classifying the landslide conditional factor values, the *LSI* was calculated progressively using equations that are adapted from other studies [25]. The FR_j was the calculated frequency ratio of a particular class of a landslide conditional factor. This evaluates the FR of the class by finding the number of landslides in the area that corresponds to the factor class interval. Equations 1 to 4 are used to calculate *LSI*:

$$FR_j = \frac{N_{Lj} N_C}{N_{Cj} N_L}$$

Equation 1

$$RF_j = \frac{FR_j}{\sum_{j=1}^{k} FR_j}$$

Equation 2

$$PR_f = \frac{RF_{jefMax} - RF_{jefMin}}{Min_g [RF_{jefMax} - RF_{jefMin}]}$$

Equation 3

$$LSI = \sum \left(RF_j \times PR_j \right)$$

Equation 4

Where:

N_{ij} is landslide pixels in class j
N_{cj} is total pixels in the class j
N_L is total landslide pixels in map
N_C is the total map pixels
RF_i is the relative frequency of the class j
RF_{jefMax} is the maximum of relative frequency in the class j of a factor f
RF_{jefMin} is the minimum of relative frequency in the class j of a factor f
$Min_g[RF_{jefMax} - RF_{jefMin}]$ is contrasts its widest RF spread with the smallest spread among all factors g
PR_f is the prediction ratio for the factor f

As noted in Section 2.2.3, selecting too many or too few classes affects map interpretability; it also influences the statistical reliability of FR weights (PR_j). When classes become overly granular, the observed/expected pixel ratios fluctuate widely, and the resulting susceptibility surface can oscillate from cell to cell [1]. At the other extreme, merging values into comprehensive classes dampens contrast and reduces a model's ability to separate landslide and non-landslide pixels [23]. The 4, 6, and 8 class sequence, therefore, represents a compromise that maintains stable *FR* estimates while preserving enough resolution to detect meaningful geomorphic variation. This forms the core of the analysis, highlighting how varying classification methods and interval ranges influence the results.

2.6 Validation of The Landslide Susceptibility Model

A robustness test determines how output variation can be attributed to various interval schemes and classification methods. The robustness test uses the *ROC* curve method to compare the success and predicting rates of the *LSI* model [14] and [26]. In addition, the training and testing data set was used as data in the *ROC* curve to produce both rates. The *ROC*-AUC analysis was carried out using the ArcGIS script tools of ArcSDM to calculate the metrics for the *LSI* maps.

ROC analysis adapted from other studies was used to compare the *LSI* map generated by each classification scheme [27]. For every threshold *t*, the true-positive rate equation 5 and false-positive rate equation 6 were computed from the 70 % training and 30 % testing subsets (where *TP* = correct landslide predictions, *FP* = false alarms, *TN* = correct non-landslide predictions, *FN* = missed landslides). Plotting *TPR* against *FPR* yields the *ROC* curve; its *AUC* quantifies model skill. Definitions follow the standard confusion-matrix terminology defined in other studies [27]. When the *LSI* is below a defined threshold, the area is defined to have no landslides. If *LSI* is above the threshold, the area is an area defined as susceptible to landslides. Similarly, suppose *LSI* indicates susceptibility to landslides for an area, which is true according to observations. The *ROC* curve is defined by plotting *TPR* vs. *FPR* obtained for different thresholds, and its *AUC* provides a single-number measure of model skill [27]. Table 4 Lists the diagnostic performance interpretation adopted in this study. Equations 5 and 6 are used to plot *ROC-AUC*:

$$TPR = \frac{TP}{TP + FN}$$

Equation 5

$$FPR = \frac{FP}{FP + TN}$$

Equation 6

Table 4: AUC ‐ based performance classes [28]

AUC range	Verbal class	Diagnostic meaning
0.90 – 1.00	Excellent	Extreme discrimination between landslide and non-landslide pixels
0.80 – 0.90	Good	Strong discrimination
0.70 – 0.80	Fair	Acceptable, but some overlap of classes
0.60 – 0.70	Poor	Limited predictive ability
< 0.50	No skill	Performance is no better than random

2.7 Zoning of LSI Maps

Landslide susceptibility mapping requires zoning the map into categories of very high to very low zones of susceptible area based on the index produced, in order to visualize the map better [29] and [30]. This study used five zones based on the landslide susceptibility level: Very low, Low, Moderate, High, and Very high zones of the susceptible area. Classification into zones again relies on statistical classification methods. The study investigates the applicability of employing the same four classification methods used for data classification: Natural breaks (Nb), Quantile breaks (Qt), Geometrical breaks (Ge), and Equal intervals (Eq) to produce applicable LS zone maps.

3. Results and Discussion

3.1 The Implication of Classification Methods on the FR Probability Distribution of a Factor

The primary aim of this work was to determine how the choice of classification scheme Natural Breaks, Quantile, Geometrical Interval, or Equal Interval influences FR landslide-susceptibility models, where FR indicates the probability of landslide susceptibility. Area (a) – Jalan Kota Batu–Subok (Table 5(a)) the slope is presented as the representative continuous factor in Table 5 because debris slides shallow, surface-controlled failures that initiate primarily on low-to-moderate gradients. All four algorithms identify the lowest-slope class as the most landslide-prone; however, the magnitude of the peak depends on the class design. Many mapped failures occur on gentle road-cuts and terrace fills, not on untouched steep slopes [9]. Because FR evaluates each variable slope separately, these anthropogenic landslides increase the slope FR wherever roads and buildings are concentrated on low gradients. Steep natural slopes, lacking such infrastructure, register fewer events and thus lower FR despite their inherent instability potential. Hence, the elevated FR in the 14–25 ° classes reflects human disturbance, not a contradiction of basic slope-stability principles. Nb and Ge isolate a narrow cluster at ≈ 14–25°; because the pixel denominator is small, the landslide count (40–43) pushes the FR to ≈ 1.5. Qt forces equal pixel counts, so its first class is wider (14–23°) yet still registers an FR of 1.47 because the numerator remains high (34 slides) while the denominator grows only modestly. Eq combines two Nb clusters into a single 14–27° class; the larger denominator dilutes the landslide concentration, yielding a similar FR (1.47) but a much higher relative frequency (0.47). Thus, the apparent "high-risk" class width and by extension the mapped hazard extent varies by up to 13° depending solely on the classification rule.

Area (b) – Jalan Jangsak–Tutong (Table 5(b)) a dual-peak pattern emerges because the slope distribution is strongly right-skewed. Eq places only 2% of pixels but four landslides (> 48.9°) in its top class, inflating FR to 2.13. Qt and Ge redistribute these extreme slopes across broader or geometrically expanding classes, reducing the FR of the same slides to ≤ 1.01. Conversely, Nb and Ge carve out a narrow low-slope class (~ 13–16°) that captures 18 landslides and yields FR ≈ 1.3; Eq merges this cluster with mid-slopes, suppressing its contribution (FR = 1.10). The contrasting peaks, therefore, stem from how each algorithm handles the sparsely populated distribution tails: algorithms that isolate the tails (Nb, Eq) exaggerate FR, whereas those that balance pixel counts (Qt) or smooth class widths (Ge) temper the extremes.

The same inventory can suggest either a single low-slope hotspot (Qt, Ge), a dual hotspot (Eq), or a muted pattern (Nb), depending strictly on class construction. Selecting a scheme that matches the study objective highlighting natural clusters, balancing sample sizes, or maintaining numeric uniformity is therefore critical to avoid misinterpreting FR outputs. Because each break method counts landslides against a different slice of slope values, the "highest-risk" band on the map shifts: Nb or Ge isolate a tight 14–25° band (Area (a)) or a very-steep tail (Area (b)) and report the highest FR, Qt spreads the cuts so the risky zone looks broader but less extreme, while Eq can overstate danger in sparse tail classes.

Table 5: FR values for slope angle in two study areas: (a) Jalan Kota Batu–Subok and (b) Jalan Jangsak–Tutong using four classification schemes (Nb, Qt, Ge, and Eq)

(a)

Classification method	Class boundaries	Landslides	Factor area (m^2)	Landslides fraction	Area fraction	Frequency ratio (FR)	Relative frequency
Natural break (Nb)	14.23 - 23.62	40	11,072,656.25	0.43	0.28	1.52	0.41
	23.63 - 33.92	31	11,361,406.25	0.33	0.29	1.14	0.31
	33.93 - 44.83	17	11,208,906.25	0.18	0.28	0.64	0.17
	44.84 - 63.91	6	5,785,312.50	0.06	0.15	0.44	0.12
Quantile break (Qt)	14.23 - 22.71	34	9,692,031.25	0.36	0.25	1.47	0.37
	22.72 - 31.20	30	9,697,812.50	0.32	0.25	1.30	0.32
	31.21 - 40.59	21	10,302,187.50	0.22	0.26	0.86	0.21
	40.60 - 63.91	9	9,736,250.00	0.10	0.25	0.39	0.10
Geometrical break (Ge)	14.23 - 24.94	43	11,989,375.00	0.46	0.30	1.50	0.37
	24.95 - 29.85	19	5,714,218.75	0.20	0.14	1.39	0.34
	29.86 - 40.56	23	11,988,437.50	0.24	0.30	0.80	0.20
	40.57 - 63.91	9	9,736,250.00	0.10	0.25	0.39	0.09
Equal interval (Eq)	14.23 - 26.65	50	14,252,187.50	0.53	0.36	1.47	0.47
	26.66 - 39.07	32	13,883,437.50	0.34	0.35	0.97	0.31
	39.08 - 51.49	11	9,195,000.00	0.12	0.23	0.50	0.16
	51.50 - 63.91	1	2,097,656.25	0.01	0.05	0.20	0.06

(b)

Classification method	Class boundaries	Landslides	Factor area (m^2)	Landslides fraction	Area fraction	Frequency ratio (FR)	Relative frequency
Natural break (Nb)	13.31 - 21.13	35	9,696,562.50	0.44	0.41	1.08	0.26
	21.14 - 29.81	21	6,964,062.50	0.26	0.29	0.90	0.22
	29.82 - 40.53	15	5,180,000.00	0.19	0.22	0.87	0.21
	40.54 - 60.79	9	2,090,468.75	0.11	0.09	1.29	0.31
Quantile break (Qt)	13.31 - 18.23	24	5,885,312.50	0.30	0.25	1.22	0.30
	18.24 - 23.73	19	6,177,812.50	0.24	0.26	0.92	0.23
	23.74 - 32.13	19	6,030,156.25	0.24	0.25	0.94	0.24
	32.14 - 60.79	18	5,837,812.50	0.23	0.24	0.92	0.23
Geometrical break (Ge)	13.31 - 15.91	18	4,207,343.75	0.23	0.18	1.28	0.31
	15.92 - 21.56	19	6,060,312.50	0.24	0.25	0.94	0.23
	21.57 - 33.90	27	8,902,187.50	0.34	0.37	0.91	0.22
	33.91 - 60.79	16	4,761,250.00	0.20	0.20	1.01	0.24
Equal interval (Eq)	13.31 - 25.18	48	13,105,781.25	0.60	0.55	1.10	0.22
	25.19 - 37.05	20	7,471,718.75	0.25	0.31	0.80	0.16
	37.06 - 48.92	8	2,791,250.00	0.10	0.12	0.86	0.18
	48.93 - 60.79	4	562,343.75	0.05	0.02	2.13	0.44

To keep decisions robust, researchers need to draw two maps one with a cluster-respecting scheme (Nb or Ge) and one with a pixel-balanced scheme (Qt) and ground-check any slope where the two disagree; avoid Eq when the data are strongly skewed, and always note the break rule and class count in project documents so the hazard map can be replicated.

3.2 The Implication of Classification Methods on Prediction Weightage Value

The application of various classification approaches, such as Nb, Qt, Ge, and Eq, is critical in distinguishing significant patterns and predictions in the analytical exploration of geographical data. As indicated by our study, which was done at two key locations: Jalan Kota Batu Subok and Jalan Jangsak Tutong, each technique, distinguished by its specific approach to classifying data into discrete groups, demonstrates differing degrees of success across different variables. In Figure 5, location (a), the prediction ratio (PR_{factor}) varies considerably with the classification method and number of classes. Under the 4-class scheme, the Qt (yellow) method produces an exceptionally high PR_{factor} for the Elevation factor, nearing a value of 9, indicating that a disproportionately large number of landslide points are concentrated within the highest quantile of this factor. This suggests that Qt, being percentile-based, can sharply highlight landslide-prone intervals when data is unevenly distributed.

However, this also reflects potential overfitting, where a narrow range of values dominates the prediction. In contrast, the Eq (brown) and Ge (green) methods show more moderate and uniform PR_{Factor}, though Eq still exhibits some inflation for factors like distance from Drain and Road at higher class counts. The Nb (orange) method tends to emphasize important contributing factors such as SPI and Settlement, providing more balanced PRs across class numbers, particularly in the 6- and 8-class schemes. Furthermore, in Jalan Jangsak-Tutong location (b) (Figure 5), both Qt (yellow) and Eq (brown) exhibit the highest PR_{factor} among all methods. Eq produces a strong *PR* peak for TRI under the 8-class scheme, while Qt displays a similarly high PR_{factor} for elevation under the 4-class scheme. These sharp increases suggest that both methods through percentile-based and fixed-interval classifications can overconcentrate landslide points in specific classes when the data is not evenly distributed. Conversely, Nb (orange) and Ge (green) methods show more moderate and balanced PR_{factor} values across most factors. Nb consistently highlights Elevation, SPI, Drain and settlement as influential factors with stable *PR* spread across all class counts. Overall, the figure illustrates that Qt and Eq are more prone to producing extreme *PR* values, whereas Nb and Ge provide smoother and more interpretable results better aligned with landslide distribution patterns. Notably, the increase in class numbers from 4 to 6 and 8 resulted in considerable changes in the Prediction ratio PR_{factor}, with certain factors exhibiting enhanced predictive power, possibly due to the detection of more subtle data variances. This discovery emphasises the importance of class number selection in investigating the precision and meaning of geographical data analysis. Prediction ratio is calculated as the *RF* spread for a factor its *max(RF) – min (RF)* divided by the minimum difference of *RF* such spread among all factors, so it rises whenever a classification scheme widens that numerator.

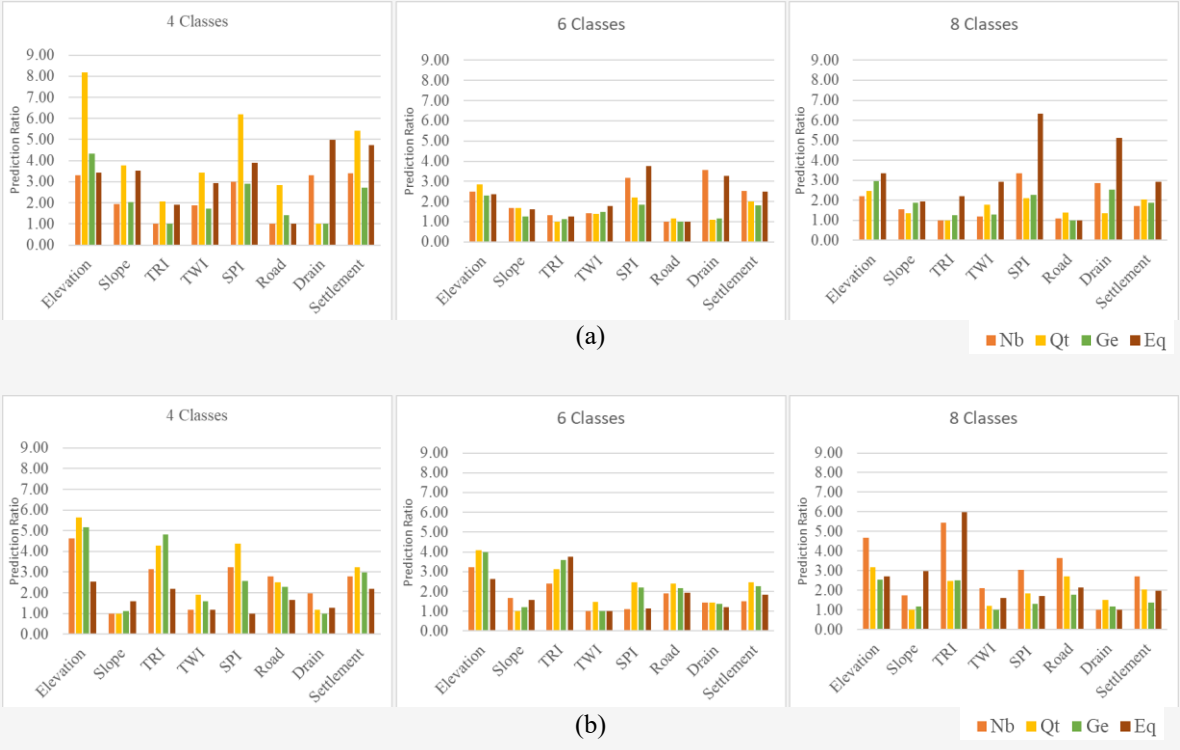

Figure 5: Prediction ratio (PRFactor) for each conditioning factor at three class counts (4, 6, 8) and four classification schemes: Nb, Qt, Ge, and Eq for: (a) Jalan Kota Batu-Subok, (b) Jalan Jangsak-Tutong

In Figure 5, Qt boost *PR* because they place class breaks at uniform data clusters: a narrow, landslide-dense tail (e.g., SPI, elevation, drain at 4 and 6 classes in case study (a); TRI and elevation at eight classes in case study (b) sits alone, while a sparsely affected tail sits at the opposite end, enlarging the max−min gap. Quantile (Qt) compresses every factor's *RF* range by forcing equal pixel counts, so it's *PR* seldom exceeds ≈3, and Equal Interval (Eq) inflates only for highly skewed variables whose

fixed-width extreme bins hold few pixels yet capture several outlier landslides. Increasing the class count from four to six often heightens the problem by separating bimodal distributions into distinct classes; adding an eighth class can fragment those clusters, shrink the *RF* Range and lowering, especially for Qt and Ge. Thus, every peak or dip in Figure 5 reflects how a particular algorithm and class number alter the numerator of the prediction-ratio formula, not a change in the intrinsic importance of the conditioning factors. It encourages a deeper understanding of the inherent qualities of data and the phenomena under research, enabling the selection of the most appropriate classification strategy, which results in more accurate and insightful predictions.

3.3 Variability in the Model Validation Analysis

The *TPR* and *FPR* have been calculated for selected uniformly distributed threshold values from 0 to 1, and the *ROC* curve has been plotted for each classification technique and each interval scheme. The current study provides a thorough examination of the LS model in two separate locations: (a) Jalan Kota Batu-Subok and (b) Jalan Jangsak-Tutong. A critical evaluation was conducted to examine the success and prediction rates of several classification methods applied in the LS model, including Nb, Qt, Ge, and Eq, as well as different class configurations (4, 6, and 8). A view of results in Table 6 is revealed when digging further into the performance of distinct classification algorithms. At location (a), the Ge and approaches excel, with success rates of 97.7% with 6 classes, respectively. In location (b), the Qt approach takes the lead, particularly for 4 and 6-class configurations, with success rates of 94.6% and 94.1%, respectively, followed by a significant performance by the Eq method at the 8-class level with a 91.8% success rate. This complicated pattern emphasizes the critical relevance of method selection in obtaining optimal accuracy, emphasizing the need to investigate the interaction between classification techniques and the complications imposed by shifting class numbers.

Furthermore, the study reveals a subtle pattern in the impact of class numbers on success and prediction rates in Table 6. There is a varied reaction to increasing class size, which contradicts the expectation of a linear rise in success or prediction rates. For example, in location (a), the Ge technique achieves a 97.7% success rate with 6 classes, but at location B, rates taper to 90.5% with 8 classes. This finding paves the way for further research into adjusting the class number to improve the model's precision and efficiency. In location (a) (Jalan Kota Batu–Subok), the predicting rates ranged from 92.20% to 96.30%, with most methods performing well above 93%. In location (b) (Jalan Jangsak–Tutong), the rates were slightly lower, ranging from 85.10% to 90.50%, showing more variability across classification methods and class numbers. *AUC* varies because each scheme partitions all 8 conditioning continuous factor layers differently. Nb and Ge place class breaks at natural data clusters, concentrating landslide-dense pixels and boosting both success and prediction *AUC*.

Table 6: Training (success) and testing (prediction) AUC values for the LS model in study area: (a) Jalan Kota Batu-Subok and (b) Jalan Jangsak Tutong, summarised by classification scheme

(a)

Classification Method	Success rates (%)			Predicting rates (%)		
	4 classes	6 classes	8 classes	4 classes	6 classes	8 classes
Nb	96.4	95.9	96.9	94.2	93.2	93.9
Qt	95.5	96.7	97.2	93.4	94.9	94.8
Ge	94.5	97.7	96.6	92.8	96.3	94.2
Eq	96.5	97.7	96.4	94.0	95.2	92.2

(b)

Classification Method	Success rates (%)			Predicting rates (%)		
	4 classes	6 classes	8 classes	4 classes	6 classes	8 classes
Nb	89.1	92.0	90.2	85.1	87.2	86.3
Qt	94.6	94.1	93.8	85.8	90.5	86.5
Ge	93.7	91.5	90.5	86.9	90.1	86.4
Eq	88.5	89.8	91.8	88.1	89.3	88.2

Qt equalises pixel counts, preventing sparsely populated tail classes and giving stable but slightly lower *AUC*, while Equal Interval can isolate only a few extreme-value pixels, inflate training *AUC* yet trim prediction *AUC*. Increasing class count from 4 to 6 improves *AUC* by separating contrasting value ranges. In contrast, an eight-class often leaves too few training pixels in the tail bin, adding variance and reducing overall accuracy. Model accuracy hinges on how the eight conditioning continuous factor layers

are discretised. Schemes that honour natural data clusters Nb and Ge concentrate landslide-dense pixels, delivering the highest and most consistent *AUC* values. Qt keeps class sizes balanced, yielding dependable but slightly lower *AUC*, whereas Eq can over-fit sparse extreme classes, boosting training accuracy yet eroding predictive skill. Moving from 4 to 6 classes sharpens contrasts and raises *AUC*, but adding an 8th class often leaves tail bins under-populated, increasing variance and diminishing overall performance.

Lastly, the study demonstrates the importance of method selection and class number optimisation in improving the performance of the LS model at various locations. The data highlights the possibility of improving prediction accuracy by gaining a more sophisticated grasp of location-specific variables and methodological interactions. Moving forward, it is crucial to delve deeper to uncover the underlying patterns that influence these trends, enabling the development of more robust and accurate prediction models. The best predicting rate in location (a) was achieved by the Ge method with 6 classes at 96.30%. In location (b), the highest predicting rate was recorded by the Qt method with 6 classes, reaching 90.50%. This suggests that the 6-class scheme, particularly under Ge and Qt methods, consistently improves model performance. These findings offer practical guidance for planners, engineers, and disaster risk managers by demonstrating how GIS-based analysis can support the development of reliable landslide susceptibility maps. By identifying the most effective classification methods and mapping strategies, the study contributes to more informed spatial planning, infrastructure design, and early warning systems in landslide-prone areas.

3.4 The Impact of the Classification Method on the Zoning System of Landslide Susceptibility Index Maps

In a different attempt, based on the highest *ROC-AUC* in Table 6, *LSI* maps of Jalan Kota Batu-Subok and Jalan Jangsak Tutong were made using a continuous dataset classified by a geometrical and quantile classification system with 6 classes. These maps were then classified into five zones using the same classification: Nb, Qt, Ge, and Eq methods to analyse the impact of classification on the *LSI* map zoning (Table 7 and Table 8). Detailed data analysis was performed in the methodical pursuit of analysing the usefulness of various zoning systems and classification schemes in forecasting landslide occurrences in the Jalan Kota Batu-Subok region in Table 7. Initially, the various zonation methods, Nb, Qt, Ge, and Eq, were examined through *LSI* Ge classification systems with 6 intervals that classify factors. The research determined that the Nb technique is cautious in forecasting landslides in the moderate zone. However, the Qt zoning method is more sensitive to landslide-prone locations, identifying a greater frequency of landslides in the very high zone. The Eq technique, on the other hand, takes a balanced approach, evenly dispersing predictions over the moderate to extremely high zones (see Table 7).

To evaluate how well each zoning scheme in the Jalan Kota Batu–Subok *LSI* map reproduces the theoretical landslide distribution proposed in previous studies [31], The study compared the observed landslide counts in each susceptibility class (very-low to very-high) with predefined target event ranges. These targets represent the expected number of landslide events per class:

a) Training dataset: (0, 0, 0–1, 5–12, >28)
b) Test dataset: (0, 0, 0–1, 2–5, >13)

Here, the two zeros correspond to the Very Low and Low zones, where no landslides are theoretically expected. The intermediate ranges (0–1, 5–12, 2–5) indicate allowable event counts in the Moderate and High zones, while the thresholds (>28, >13) specify the minimum required number of events in the Very High zone (Table 7).

Gaps in the ranges (e.g., no values between 2–4 in the training dataset) reflect that no events are expected within those intervals, not an omission of data. Among the classification methods, the Quantile (Qt) scheme produced the closest match to these targets, allocating 89 (training) and 39 (test) landslides to the Very High zone well above the required thresholds while keeping intermediate class allocations within one event of their targets. Other schemes either under-allocated landslides to the Very High zone or spread them more broadly across Moderate and High classes, reducing alignment with the theoretical distribution. This strong alignment shows that Qt preserves the empirical frequency structure of the inventory better than the other methods and therefore provides the most efficient baseline for developing more refined landslide-prediction models in the corridor.

Table 7: Landslide counts by susceptibility zone based on Ge six-class classification for Jalan Kota Batu–Subok

Zonation method	LS zones	Training dataset	Testing dataset
Nb	Very Low	0	0
	Low	1	0
	Moderate	3	1
	High	21	7
	Very High	69	32
Qt	Very Low	0	0
	Low	1	0
	Moderate	1	0
	High	3	1
	Very High	89	39
Ge	Very Low	0	0
	Low	3	0
	Moderate	1	1
	High	12	7
	Very High	78	32
Eq	Very Low	0	0
	Low	1	0
	Moderate	10	3
	High	62	30
	Very High	21	7

Table 8: Landslide counts by susceptibility zone based on Qt six-class classification for Jalan Jangsak–Tutong

Zonation method	LS zones	Training dataset	Testing dataset
Nb	Very Low	0	0
	Low	0	0
	Moderate	4	2
	High	19	12
	Very High	57	21
Qt	Very Low	0	0
	Low	1	1
	Moderate	3	1
	High	14	10
	Very High	61	23
Ge	Very Low	0	0
	Low	0	0
	Moderate	2	0
	High	16	9
	Very High	61	26
Eq	Very Low	0	0
	Low	0	0
	Moderate	4	2
	High	49	22
	Very High	26	11

Equal zonation methods place fewer landslide points in the Very High zones (21 and 7 landslides) because they divide susceptibility values or map areas uniformly without considering the actual distribution of landslides. As a result, landslide-prone areas may be spread across multiple zones, reducing the concentration in the highest-risk class. In contrast, data-driven methods like natural breaks or quantiles group values based on landslide density, leading to better capture of landslide points in the Very High zone.

For the Jalan Jangsak–Tutong area (Table 8), the expected landslide event ranges based on previous studies [31], were:

a) Training dataset: (0, 0, 0–1, 4–10, >27)
b) Test dataset: (0, 0, 0, 2–4, >12)

Zeros again indicate no expected landslides in Very Low and Low zones. The intermediate ranges show the allowable landslide counts in the Moderate and High zones, and the ">" values specify the minimum number of events required in the Very High zone. A detailed comparison (Table 8) showed that Qt and Ge methods aligned most closely with these theoretical ranges, particularly in the Very High zone, where both classified 61 training landslides and over 21 test landslides well above the required thresholds. Eq, in contrast, spread more landslides into the High zone while underestimating Very High counts. Overall, Qt and Ge closely match the expected landslide event ranges based on previous studies [31] by placing most landslides in the Very High zone. Nb moderately aligns but shows inflated counts in Moderate and High zones. Eq performs the least accurately, underestimating Very High zone counts and overpopulating the High zone, which may weaken the map's risk prioritisation. These insights pave the way for further refined research in enhancing the accuracy of predictive models in identifying landslide-prone areas in the region. This insight is highly beneficial for planners, engineers, and disaster risk managers, as it reinforces the importance of using empirically validated classification strategies to improve the reliability of hazard zoning maps. Although the Qt method performed best in this study, the findings highlight that classification suitability is context dependent. Therefore, it is recommended that end-users evaluate multiple classification methods to identify the most effective approach for their specific study area and data characteristics.

3.5 The Impact of Classification on Map Visualization

A comprehensive visual assessment of the generated maps was conducted to evaluate their suitability for identifying landslide (LS) zones. Figure 6(a) illustrates the LS zone maps for the Jalan Kota Batu–Subok region, produced using the *LSI* map based on the Ge approach with six-interval factor classifications. This approach was selected because it yielded the highest *ROC–AUC* results (see Table 6(a)), indicating strong capability in classifying actual landslide points. Similarly, the *LSI* map for the Jalan Jangsak–Tutong region was generated using the Qt approach with six-interval factor classifications, also chosen due to the highest *ROC–AUC* results (see Table 6(b)) demonstrating comparable classification performance. Figures 7 and 8 present the visual zonation and percentage distribution of landslide susceptibility in the Jalan Kota Batu–Subok area, while Figures 9 and 10 display the corresponding zonation and distribution for the Jalan Jangsak–Tutong region. The *LSI* map itself in Figure 6(a) displays a green-red gradient from low (38.85) to high (590.89) susceptibility values, serving as the base raster for reclassification. The six-interval classification method produced an *LSI* map where high susceptibility values (red) are more localized compared to the broader distribution of moderate and low values. The narrower range of high *LSI* values suggests that reclassification into susceptibility zones will generate a more concentrated high-risk zone.

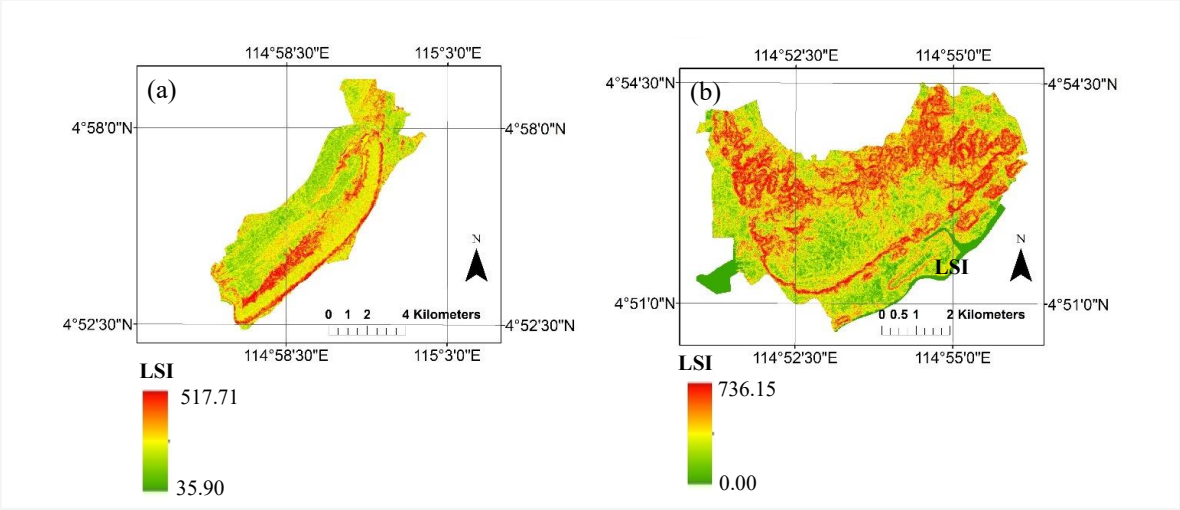

Figure 6: Landslide susceptibility index: (a) Jalan Kota Batu–Subok. (b) Jalan Jangsak–Tutong

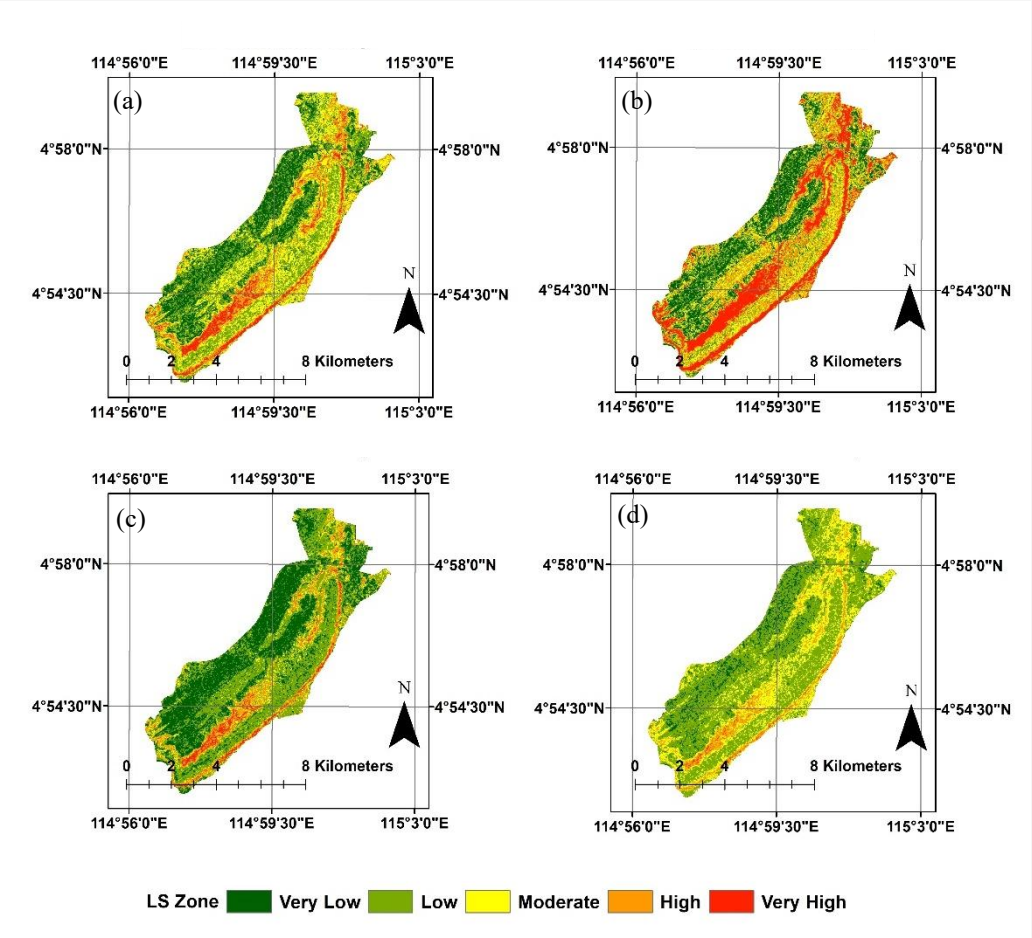

Figure 7: LSI maps derived from Geometrical classification methods with 6 classes classification for Jalan Kota Batu–Subok: (a) natural breaks (b) quantile (c) geometrical interval (d) equal interval zonations

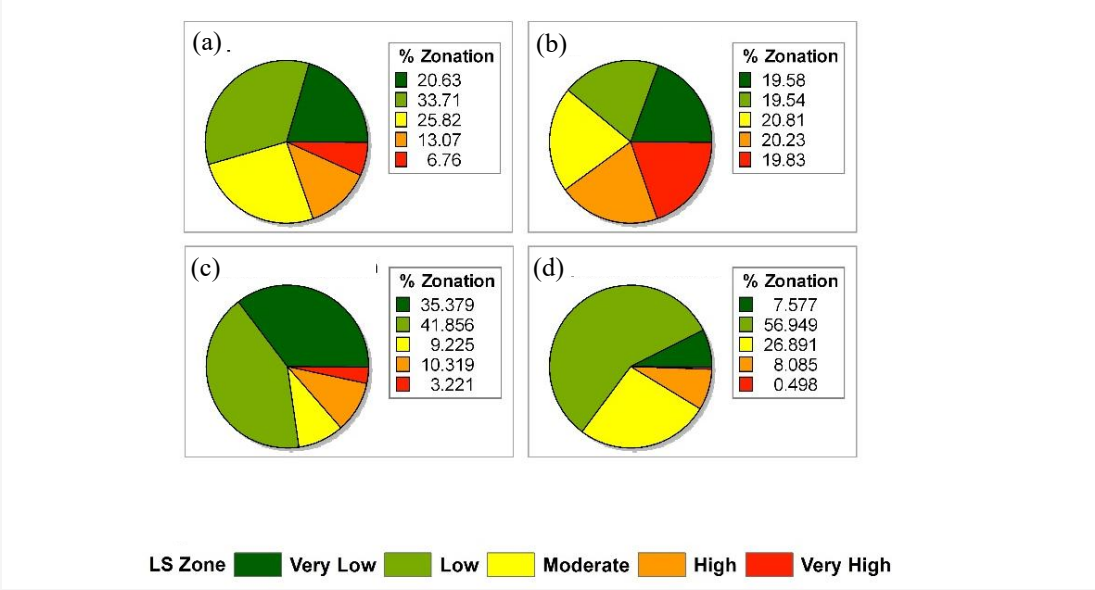

Figure 8: Variations of LSI zones derived from different classification methods with Ge 6 classes for Jalan Kota Batu–Subok: (a) natural breaks (b) quantile (c) geometrical interval (d) equal interval

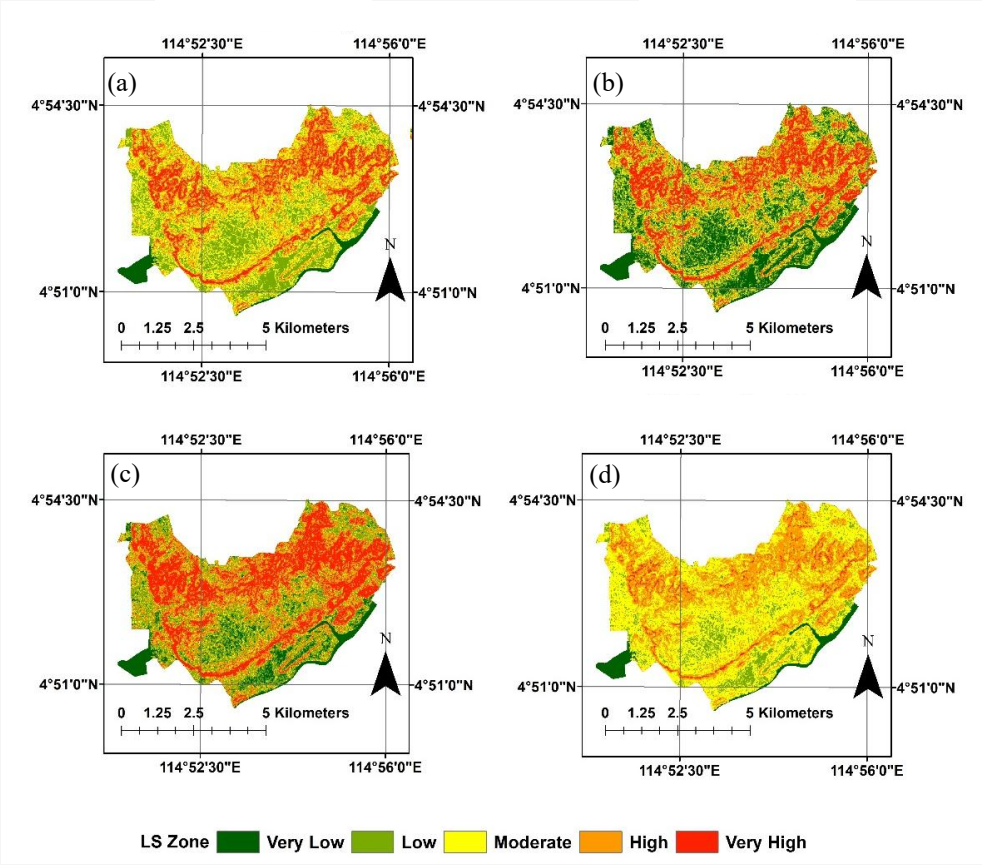

Figure 9: LSI maps derived from Quantile classification methods with 6 classes classification for Jalan Jangsak Tutong: (a) natural breaks (b) quantile (c) geometrical interval (d) equal interval zonation

This indicates that the selected classification approach effectively differentiates areas within the dataset, ensuring that the subsequent susceptibility zoning reflects the underlying LSI value distribution accurately.

All methods consistently identify high and very high susceptibility zones along the central and eastern terrain, while western areas predominantly fall under low to very low categories (Figure 7). However, spatial variations emerge across methods: Nb highlights abrupt susceptibility transitions with irregular boundaries, Qt emphasizes equal pixel counts per class, often enlarging high-risk zones, Ge provides smoother gradations with balanced representation between classes, and Eq applies uniform intervals, sometimes underestimating localized high-risk areas. These variations demonstrate how classification methods influence susceptibility mapping and highlight the need for careful selection when supporting hazard planning and decision-making. The accompanying pie charts in Figure 8 illustrate the percentage of area occupied by each susceptibility class under each classification method. Nb classification results in a relatively balanced distribution, dominated by Low (33.71%) and Moderate (26.82%) zones. Qt produces an almost equal distribution across all five zones (approximately 20% each), due to its percentile-based design. Ge classification emphasizes the lower risk zones, with 41.86% and 35.38% of the area falling into Low and Very Low zones, respectively. The Eq method shows a strong bias toward lower zones, placing 56.95% of the area in Low and only 0.5% in the Very High category.

The *LSI* map in Figure 6(b), rendered in green-red gradient, represents raw susceptibility values ranging from 0 to 759.31. LSI map shows a wider spread of high LSI values across the study area. The broader distribution reflects greater variation within the raw LSI data, meaning that the same six-interval classification will likely produce a different zonation pattern compared to Jalan Kota Batu–Subok. This highlights the importance of the classification method in standardizing outputs across study areas with differing data characteristics, ensuring comparability when interpreting final susceptibility zones.

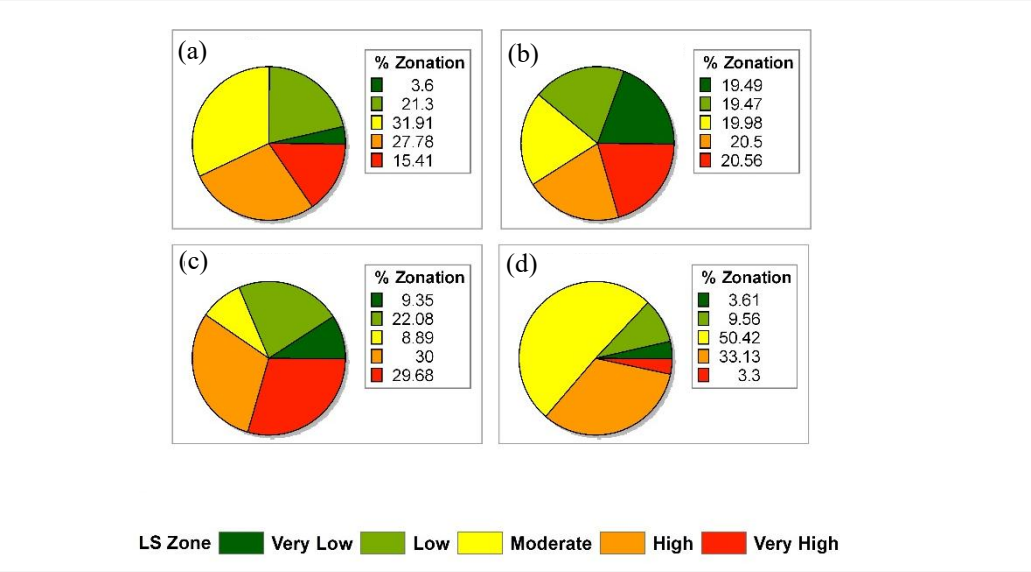

Figure 10: Variations of LSI zones derived from different classification methods with Qt 6 classes for Jalan Jangsak Tutong: (a) natural breaks (b) quantile (c) geometrical interval (d) equal interval

According to Figure 9, while all methods consistently identify the northern and northeastern hills as high-risk areas, Qt tends to inflate the very high-risk zones because it forces equal pixel counts per class, potentially overemphasizing hazard areas where landslide evidence may be sparse. Nb, by contrast, responds to natural data clusters, highlighting localized hotspots but sometimes fragmenting risk zones, which might complicate mitigation planning. Ge strikes a balance by controlling for extreme values and producing smoother transitions, making it suitable for regional-scale planning where both detail and interpretability matter. Meanwhile, Eq often compresses most pixels into mid-risk classes, diluting the contrast between stable and unstable slopes, which risks underestimating high-risk terrain in hazard-sensitive areas. These differences underscore that classification is not merely a visualization step but a decision-making variable an inappropriate choice can either inflate mitigation costs or understate true hazard exposure, directly influencing land-use planning, resource allocation, and community risk perception. Based on Figure 10, under the Nb classification, most of the area is categorized as Moderate (31.91%) and High (27.78%), with Very High occupying 15.41%. The Qt method distributes the area more evenly, with each class covering approximately 19–21%. Ge classification places most of the area in High (29.68%) and Moderate (30%) zones. In comparison, Eq classification shows a strong dominance of the Moderate class (50.42%), with only 3.3% of the area classified as Very High.

The differing behaviours of the classification methods Nb, Qt, Ge, and Eq stem from their underlying mathematical principles and how they divide the continuous *LSI* values into discrete classes. Nb identifies breakpoints based on natural groupings in the data, minimizing within-class variance and maximizing between-class variance. This often results in a balanced distribution but can also reflect dominant groupings in the data, leading to clusters in specific classes like Low or Moderate. Qt, on the other hand, ensures that each class contains an equal number of pixels, resulting in a nearly uniform distribution of area across all five zones (approximately 20% each), regardless of the actual spread of *LSI* values.

Ge classification uses exponentially increasing intervals, making it particularly suited for skewed data. When *LSI* values are concentrated in the lower range, Ge tends to assign a large portion of the area to Very Low and Low classes. Meanwhile, the Eq method divides the entire *LSI* range into equal-sized numeric bands, which can skew results toward the middle if data values are unevenly distributed. This explains why Eq often shows a strong dominance of the Moderate or Low class and only a small portion in the Very High category. Overall, each method interacts differently with the data distribution, influencing the spatial extent of susceptibility zones and highlighting the importance of selecting a classification approach aligned with the map's intended interpretation. This study underscores that the choice of classification method plays a critical role in shaping the visual and statistical representation of landslide susceptibility maps.

These variations highlight that no single method is universally optimal classification schemes must be selected and justified based on the data characteristics and intended use of the susceptibility map. For planners, engineers, and risk managers, this means classification decisions should be made with an awareness of how they influence hazard communication, priority setting, and mitigation planning.

4. Conclusion

This study shows that discretisation choices alone Nb, Qt, Ge, and Eq at 4, 6, and 8-class splits can shift testing AUC for FR landslide-susceptibility models from 85% to 96% and reposition "Very-High" hazard belts by up to 15 % of study area, with Nb and Ge excelling where landslide clusters are tight, Qt smoothing class imbalance, and Eq occasionally inflating sparsely populated tails; hence no single scheme is universally optimal and practitioners should run at least an Nb (or Ge) versus Qt sensitivity pair and investigate zones where the two maps disagree. Limitations include the absence of high-resolution rainfall data, single-run AUC values that preclude significance testing, and a decade-long inventory that may miss low-frequency deep failures. Future work should adopt a standard four-step workflow: (1) require core inputs ≤10 m DEM, inventory, and key conditioning layers; (2) run two benchmark LSI maps automatically a cluster-respecting Nb/Ge-6 class and a pixel-balanced Qt-6 class and flag areas where they disagree; (3) publish the full confusion matrix, $ROC - AUC$, and zone-overlap metric; and. An open-source Python/ArcPy toolbox can automate these steps, making landslide-susceptibility mapping reproducible and scalable across regions. While the prediction ratio provides a pair-wise weighting that highlights how strongly each factor differentiates landslide and non-landslide pixels relative to the others, it does not model true cross-factor interactions (e.g., "steep slope × shallow soil × proximity to road"). We therefore acknowledge that the FR framework, even with prediction-ratio weighting, still evaluates factors independently; complex, multi-variable synergies may be under-represented. Future work will benchmark these FR results against multivariate or machine-learning approaches that can capture such interaction effects explicitly. In addition, because the analysis relies on a 12.5 m DEM, failures smaller than ~30 m may be under-resolved; future work should repeat the workflow with ≤ 2 m LiDAR to test model performance at finer scales.

Acknowledgments

The authors would like to thank the Public Works Department of Brunei (Geotechnical and Research Section, Department of Technical Services), Agricultural Department of Brunei, Universiti Teknologi Brunei, Brunei Darussalam for providing the enabling environment that facilitated this research. The research is funded under the education scheme for postgraduate studies by the Ministry of Education, Brunei Darussalam.

References

[1] Wubalem, A., (2021). Landslide Susceptibility Mapping Using Statistical Methods in Uatzau Catchment Area, Northwestern Ethiopia. *Geoenvironmental Disasters*, 1–21. https://doi.org/10.1186/s40677-020-00170-y.

[2] Wang, J., Wang, Y., Li, C., Li, Y. and Qi, H., (2024). Landslide Susceptibility Evaluation Based on Landslide Classification and ANN-NFR Modelling in the Three Gorges Reservoir Area, China. *Ecological Indicators*, Vol. 160. https://doi.org/10.1016/j.ecolind.2024.111920.

[3] Moreira, L. L., Brito, M. M. de and Kobiyama, M., (2021). Effects of Different Normalization, Aggregation, and Classification Methods on the Construction of Flood Vulnerability Indexes. *Water*, Vol. 13, 7–9. https://doi.org/10.3390/w13010098.

[4] Yatim Mustapa, M., and Tahar, K. (2025). Landslide Susceptibility Mapping Utilizing the Weighted Frequency Ratio Technique: A Case Study of Klang Valley, Malaysia. *International Journal of Geoinformatics*, Vol. 21(2), 70–86. https://doi.org/10.52939/ijg.v21i2.3939.

[5] Thammaboribal, P., Triapthti, N., and Lipiloet, S. (2025). Using of Analytical Hierarchy Process (AHP) in Disaster Management: A Review of Flooding and Landslide Susceptibility Mapping. *International Journal of Geoinformatics*, Vol. 21(4), 177–196. https://doi.org/10.52939/ijg.v21i4.4091.

[6] Karakas, G., Unal, E. O., Cetinkaya, S., Ozcan, N. T., Karakas, V. E., Can, R., Gokceoglu, C. and Kocaman, S., (2024). Analysis of Landslide Susceptibility Prediction Accuracy with an Event-Based Inventory: The 6 February 2023 Turkiye Earthquakes. *Soil Dynamics and Earthquake Engineering*, Vol. 178. https://doi.org/10.1016/j.soildyn.2024.108491.

[7] Sinčić, M., Bernat Gazibara, S., Rossi, M. and Mihalić Arbanas, S., (2025). Comparison of Conditioning Factor Classification Criteria in Large-Scale Statistically Based Landslide Susceptibility Models. *Natural Hazards and Earth System Sciences*, Vol. 25, 183–206. https://doi.org/10.5194/nhess-25-183-2025.

[8] Geotechnical Department Unit, Public Works Department Brunei Darussalam. (2019). *Landslide and Rainfall Data 2008–2018* (Unpublished internal report, Excel dataset). Bandar Seri Begawan: Public Works Department.

[9] Sahari, S. N. R. J. S. and Batmanathan, A. A. S. N., (2021). Preliminary Analysis of Landslide Hazard in Brunei Darussalam, SE Asia. *Environmental Earth Sciences*, Vol. 80, 1–16. https://doi.org/10.1007/s12665-021-09815-z.

[10] Geotechnical Department Unit, Public Works Department Brunei Darussalam. (2022). *Landslide Pictures of Case Studies Area* (Unpublished internal report, photographic dataset). Bandar Seri Begawan: Public Works Department.

[11] NASA ASF Data Search Vertex. (n.d.). *Earth Data*. [Online]. Available: https://search.asf .alaska.edu. [Accessed: Nov. 23, 2023].

[12] Pradhan, B., Naemah, M. and Abdullahi, S., (2017). Spatial Prediction of Landslides along Jalan Kota in Bandar Seri Begawan (Brunei) Using Airborne LiDAR Data and Support Vector Machine. *Laser Scanning Applications in Landslide Assessment*, Springer. 1–359. https://doi.org/10.1007/978-3-319-55342-9

[13] Saravanan, S., Istijono, B., Jennifer, J.J., Abijith, D. and Sivaranjani, S., (2021). Landslide Susceptibility Assessment Using Frequency Ratio Technique – A Case Study of NH67 Road Corridor in the Nilgiris District, Tamilnadu, India. *IOP Conference Series: Earth and Environmental Science*, Vol. 708. https://doi.org/10.1088/1755-1315/708/1/012 017.

[14] Berhane, G., Kebede, M., Alfarah, N., Hagos, E., Grum, B., Giday, A., Gebremedhin, K., Tsegay, T. and Tekle, T., (2020). Landslide Susceptibility Zonation Mapping Using GIS-Based Frequency Ratio Model with Multi-Class Spatial Data-Sets in the Adwa-Adigrat Mountain Chains, Northern Ethiopia. *Journal of African Earth Sciences*, Vol. 164. https://doi. org/10.1016/j.jafrearsci.2020.103795.

[15] Ozioko, O. H. and Igwe, O., (2020). GIS-Based Landslide Susceptibility Mapping Using Heuristic and Bivariate Statistical Methods for Iva Valley and Environs Southeast Nigeria. *Environmental Monitoring and Assessment*, Vol. 192. https://doi.org/10.1007/s10661-019-7951-9.

[16] Hendraya, Y., Amirul, F. Y., Muhamad, A., Erizal, E., Suria Darma, T. and Ery, S., (2025). The Pore Water Pressure Changes on Forested Slopes in Tropical Humid Climate Area. *Journal of Ecological Engineering*, Vol. 26, 121–136. https://doi.org/10.12911/22998993/1 95428.

[17] Qasimi, A. B., Isazade, V., Enayat, E., Nadry, Z. and Majidi, A. H., (2023). Landslide Susceptibility Mapping in Badakhshan Province, Afghanistan: A Comparative Study of Machine Learning Algorithms. *Geocarto International*, Vol. 38. https://doi.org/10.1080/ 10106049.2023.2248082.

[18] Jiang, B., (2013). Head/Tail Breaks: A New Classification Scheme for Data with a Heavy-Tailed Distribution. *Professional Geographer,* Vol. 65, 482–94. https://doi.org/10.1080/003 30124.2012.700499.

[19] Kaye, N. R., Hartley, A. and Hemming, D., (2012). Mapping the Climate: Guidance on Appropriate Techniques to Map Climate Variables and their Uncertainty. *Geoscientific Model Development*, Vol. 5, 245–56. https://doi.org/10.5194/gmd-5-245-2012.

[20] Shao, X., Ma, S., Xu, C., Zhang, P., Wen, B., Tian, Y., Zhou, Q. and Cui, Y., (2019). Planet Image-Based Inventorying and Machine Learning-Based Susceptibility Mapping for the Landslides Triggered by the 2018 Mw6.6 Tomakomai, Japan Earthquake. *Remote Sensing*, Vol. 11. https://doi.org/10.3390/rs11 080978.

[21] Kamal, A., Dhakal, P., Javaid, A. Y., Devabhaktuni, V. K., Kaur, D., Zaientz, J. and Marinier, R., (2021). Recent Advances and Challenges in Uncertainty Visualization: A Survey. *Journal of Visualization*, Vol. 24, 861–90. https://doi.org/10.1007/s12650-021-00755-1.

[22] Anderson, C. L. and Robinson, A. C., (2022). Affective Congruence in Visualization Design: Influences on Reading Categorical Maps. *IEEE Transactions on Visualization and Computer Graphics*, Vol. 28, 2867–78. https://doi.org/ 10.1109/TVCG.2021.3050118.

[23] Cantarino, I., Carrion, M. A., Martínez-Ibáñez, V. and Gielen, E., (2023). Improving Landslide Susceptibility Assessment Through Frequency Ratio and Classification Methods -Case Study of Valencia Region (Spain). *Applied Sciences (Switzerland)*, Vol. 13. https://doi.org/10.3390/app13085146.

[24] Razavizadeh, S., Solaimani, K., Massironi, M. and Kavian, A., (2017). Mapping Landslide Susceptibility with Frequency Ratio, Statistical Index, and Weights of Evidence Models: A Case Study in Northern Iran. *Environmental Earth Sciences*, Vol. 76. https://doi.org/10.1007/s12665-017-6839-7.

[25] Youssef, B., Bouskri, I., Brahim, B., Kader, S., Brahim, I., Abdelkrim, B. and Spalević, V., (2023). The Contribution of the Frequency Ratio Model and the Prediction Rate for the Analysis of Landslide Risk in the Tizi N'tichka Area on the National Road (RN9) Linking Marrakech and Ouarzazate. *Catena*, Vol. 232. https://doi.org/10.1016/j.catena.2023.107464.

[26] Wubalem, A. and Meten, M., (2020). Landslide Susceptibility Mapping Using Information Value and Logistic Regression Models in Goncha Siso Eneses Area, Northwestern Ethiopia. *Discover Applied Sciences*. https://doi.org/10.1007/s42452-020-2563-0.

[27] Marko, S., Bernat Gazibara, S., Rossi, M. and Mihalić Arbanas, S., (2025). Comparison of Conditioning Factor Classification Criteria in Large-Scale Statistically Based Landslide Susceptibility Models. *Natural Hazards and Earth System Sciences*, Vol. 25, 183–206. https://doi.org/10.5194/nhess-25-183-2025.

[28] Dou, J., Yunus, A. P., Bui, D. T., Merghadi, A., Sahana, M., Zhu, Z., Chen, W., Han, Z. and Pham, B. T., (2020). Improved Landslide Assessment Using Support Vector Machine with Bagging, Boosting, and Stacking Ensemble Machine Learning Framework in a Mountainous Watershed, Japan. *Landslides*, Vol. 17, 641–658. https://doi.org/10.1007/s10346-019-01286-5.

[29] Temme, A. J. A. M., (2021). Relations Between Soil Development and Landslides. *Hydrogeology, Chemical Weathering, and Soil Formation*, 177–85. https://doi.org/10.1002/9781119563952.ch9.

[30] Wang, Z., Wang, D., Guo, Q. and Wang, D., (2020). Regional Landslide Hazard Assessment through Integrating Susceptibility Index and Rainfall Process. *Natural Hazards*, Vol. 104, 2153–73. https://doi.org/10.1007/s11069-020-04265-5.

[31] Kmenta, S. and Ishii, K., (2000). Scenario-Based FMEA: A Life Cycle Cost Perspective. *International Design Engineering Technical Conferences and Computers and Information in Engineering Conference*, 163–73. https://doi.org/10.1115/detc2000/rsafp-14478.